Biofabrication

International Society for Biofabrication

ACCEPTED MANUSCRIPT

Decellularized tissue exhibits large differences of extracellular matrix properties dependent on decellularization method: novel insights from a standardized characterization on skeletal muscle

To cite this article before publication: Lisanne Terrie *et al* 2024 *Biofabrication* in press https://doi.org/10.1088/1758-5090/ad2c99

Manuscript version: Accepted Manuscript

Accepted Manuscript is "the version of the article accepted for publication including all changes made as a result of the peer review process, and which may also include the addition to the article by IOP Publishing of a header, an article ID, a cover sheet and/or an 'Accepted Manuscript' watermark, but excluding any other editing, typesetting or other changes made by IOP Publishing and/or its licensors"

This Accepted Manuscript is © **2024 IOP Publishing Ltd**.

During the embargo period (the 12 month period from the publication of the Version of Record of this article), the Accepted Manuscript is fully protected by copyright and cannot be reused or reposted elsewhere.

As the Version of Record of this article is going to be / has been published on a subscription basis, this Accepted Manuscript will be available for reuse under a CC BY-NC-ND 3.0 licence after the 12 month embargo period.

After the embargo period, everyone is permitted to use copy and redistribute this article for non-commercial purposes only, provided that they adhere to all the terms of the licence https://creativecommons.org/licences/by-nc-nd/3.0

Although reasonable endeavours have been taken to obtain all necessary permissions from third parties to include their copyrighted content within this article, their full citation and copyright line may not be present in this Accepted Manuscript version. Before using any content from this article, please refer to the Version of Record on IOPscience once published for full citation and copyright details, as permissions may be required. All third party content is fully copyright protected, unless specifically stated otherwise in the figure caption in the Version of Record.

View the article online for updates and enhancements.

This content was downloaded from IP address 134.58.253.56 on 08/03/2024 at 16:39

IOP Publishing Journal Title
Journal **XX** (XXXX) XXXXXX https://doi.org/XXXX/XXXX

Decellularized tissue exhibits large differences of extracellular matrix properties dependent on decellularization method: novel insights from a standardized characterization on skeletal muscle

Lisanne Terrie[1,#], Charlot Philips[1,#], Ewout Muylle[1], Antoine Weisrock[1,2], Pauline Lecomte-Grosbras[2] and Lieven Thorrez[1]

[1] Tissue Engineering Lab, Department of Development and Regeneration, KU Leuven, Kortrijk, Belgium
[2] Univ. Lille, CNRS, Centrale Lille, UMR 9013 - LaMcube - Laboratoire de Mécanique, Multiphysique, Multi-échelle, Lille, France
[#] These authors contributed equally to this work.

E-mail: lieven.thorrez@kuleuven.be

Abstract

BACKGROUND: Decellularized matrices are an attractive choice of scaffold in regenerative medicine as they can provide the necessary extracellular matrix (ECM) components, signals and mechanical properties. Various detergent-based protocols have already been proposed for decellularization of skeletal muscle tissue. However, a proper comparison is difficult due to differences in species, muscle origin and sample sizes. Moreover, a thorough evaluation of the remaining acellular matrix is often lacking.

METHODS: We compared an in-house developed decellularization protocol to four previously published methods in a standardized manner. Porcine skeletal muscle samples with uniform thickness were subjected to in-depth histological, ultrastructural, biochemical and biomechanical analysis. In addition, 2D and 3D cytocompatibility experiments were performed.

RESULTS: We found that the decellularization methods had a differential effect on the properties of the resulting acellular matrices. Sodium deoxycholate combined with DNase I was not an effective method for decellularizing thick skeletal muscle tissue. Triton X-100 in combination with trypsin, on the other hand, removed nuclear material but not cytoplasmic proteins at low concentrations. Moreover, it led to significant alterations in the biomechanical properties. Finally, sodium dodecyl sulphate (SDS) seemed most promising, resulting in a drastic decrease in DNA content without major effects on the ECM composition and biomechanical properties. Moreover, cell attachment and metabolic activity were also found to be the highest on samples decellularized with SDS.

CONCLUSIONS: Through a newly proposed standardized analysis, we provide a comprehensive understanding of the impact of different decellularizing agents on the structure and composition of skeletal muscle. Evaluation of nuclear content as well as ECM composition, biomechanical properties and cell growth are important parameters to assess. SDS comes forward as a detergent with the best balance between all measured parameters and holds the most promise for decellularization of skeletal muscle tissue.

Keywords: Skeletal muscle, decellularization, porcine, tissue engineering, extracellular matrix, detergent

Accepted Manuscript

 © xxxx IOP Publishing Ltd

1. Background

Skeletal muscle comprises around 40% of total human body mass and is thus the most abundant tissue in the human body. A defining characteristic of skeletal muscle is its remarkable capacity for regeneration. This occurs through a highly orchestrated process which can be divided into interrelated and time-dependent phases (1). However, in so-called volumetric muscle loss (VML) the damage is too extensive for normal healing to cope with and surgical interventions are warranted. Such large skeletal muscle injuries may result from a variety of events, including direct trauma (such as motor vehicle accidents, tumor ablation surgeries, surgical debridement secondary to injuries or battlefield extremity traumas) and indirect causes (such as ischemia, infection or neurological dysfunction). Regardless of the cause, failure of the muscle to regenerate properly can have a severe impact on an individual's quality of life due to the onset of chronic functional deficits (2). Unfortunately, surgical reconstruction with myocutaneous free tissue flaps hardly achieves full regeneration of the lost muscle tissue or aesthetic reconstruction and often leads to donor site morbidity (3).

Given the variety of causes and the widespread incidence but the lack of an effective therapy, the development of new therapeutic strategies to treat severe skeletal muscle injuries is warranted. In the field of regenerative medicine, tissue engineering strategies are used to recreate tissue for transplantation. This entails seeding of cells on scaffolds which are mimicking the extracellular matrix (ECM) environment. Although the initial role of the scaffold during muscle tissue engineering applications is to give a three-dimensional supportive space to the cells, the crucial role of the ECM *in vivo* stretches beyond providing structural support (4). Indeed, increasing evidence shows the role of ECM in the development (5), function (4) and repair of muscles (6). And thus, the native ECM can be considered as a blueprint for synthetic scaffold designs. However, given the complexity of the ECM composition, it is unlikely that the current synthetic materials represent the full spectrum of ECM molecules present in skeletal muscle tissue. ECM of native muscle without the cells is a highly interesting alternative to synthetic scaffolds since the remaining matrix retains the desired structure and composition. Moreover, the innate vasculature and nervous system embedded within the ECM can be preserved as well, which are both crucial for future integration with the host tissue. Therefore, decellularization methods to remove the cells from muscle tissue, ideally without affecting the ECM, have been developed by several groups.

Various immersion decellularization protocols have been applied to skeletal muscle and differ in several aspects which complicates a proper comparison. In most cases, efficient decellularization is obtained by combining different chemical, enzymatic and/or physical agents. A recurrent combination is the use of the detergent sodium deoxycholate (SDC) and the enzyme deoxyribonuclease I (DNase I). This combination was shown to be successful for decellularizing rabbit diaphragm (7) and rat abdominal wall muscle tissue (8,9). However, when compared to a protocol based on the combination of trypsin, EDTA, Triton and NH_4OH, SDC combined with DNase I was shown to be less effective in removing all cellular material and maintaining the ECM structure (10).

Comparable results were reported by Naik *et al*., who stated that SDC combined with DNase I was insufficient to decellularize 4 x 1 x 1 cm samples of human masseter and zygomaticus major muscle (11). In this paper, a detergent-only treatment with 2% sodium dodecyl sulphate (SDS) was found to be optimal for decellularizing both zygomaticus major and masseter muscle. However, it has been described that 2% SDS significantly affects the ultrastructure of the ECM matrix when applied to rabbit cricoarytenoid dorsalis muscle (12). In addition to this, others have tested additional SDS concentrations and exposure times and combinations with Triton or enzymes on different muscles from a variety of species (13–15). However, SDS treatment often results in a significant loss of collagen and glycosaminoglycans (GAGs) and thus protocols replacing SDS with the milder detergent Triton X-100 emerged. Again, a variety of combinations and concentrations have been evaluated in rat (16–18), porcine (19) and even human tissues (10). Another combination of enzymatic (trypsin) and chemical decellularization agents (chloroform/methanol, SDC, Triton, peracetic acid/ethanol) was described by the group of Wolf *et al*. on dog quadriceps and hamstring muscles (20). The muscle-derived ECM scaffold was shown to be thoroughly decellularized while preserving most of the components found in native ECM, however these results were only described for 2.25 mm thick sheets of muscle.

Taken together, to date, many of the described immersion decellularization protocols are either insufficient to obtain thick (>1 mm) acellular matrices or damage the tissue structure upon cellular material removal. And thus, the need to further optimize immersion decellularization protocols still exists. An important difference among the various protocols in literature is the sample thickness. Often thickness varies or dimensions are not well defined. Also, the variety in muscle origin, species and evaluation criteria makes it difficult to define the best protocol based on a literature search. In this study, we selected five protocols, covering the most frequently used protocols. Decellularization efficiency was evaluated based on DNA stainings, gel electrophoresis and a DNA quantification assay. Matrix evaluation was based on several histological stainings combined with quantitative

Accepted Manuscript

assays for collagen and GAG retention, scanning electron microscopy (SEM) imaging and uniaxial tensile testing. Finally, cytocompatibility was also assessed both in 2D and 3D. With this, we provide a multi-faceted standardized analysis, which aids in selecting a suitable protocol for decellularizing thick skeletal muscle tissue.

2. Materials and methods

2.1 Tissue harvesting

Porcine skeletal muscle was harvested as residual tissue from the biceps femoris of freshly euthanized pigs (13-16 weeks old, 50-60 kg, male, cross breed between Large White and Landrace) (Orsi Academy) and stored in high glucose Dulbecco's Modified Eagle Medium (Gibco; 31966021) at 4 °C for a maximum storage time of 18 h. All protocols were conducted using samples pooled from three distinct pigs. The sample numbers correspond to different muscle samples randomly selected from this pool of three pigs. Harvested tissue was cut in beam-shaped samples of 5 x 5 x 20 mm and kept at -80 °C until further use. For mechanical testing, length of the samples was increased to 4 cm to have 2 cm of tissue between the clamps of the testing device.

2.2 Decellularization of skeletal muscle tissue

Skeletal muscle was decellularized through the application of five different protocols, of which four were selected from the literature and one in-house protocol. Untreated skeletal muscle tissue served as the native control group. For each decellularization protocol, 32 samples were decellularized and all steps were performed under continuous agitation.

Protocol n.1 was applied as described by Porzionato *et al*. (10). Briefly, samples were washed with distilled water for 24 h at 4 °C. Next, samples were incubated for 1 h with 0.05% trypsin-0.02% EDTA (Gibco; 25300054) at 37 °C. Following a short washing step in PBS at room temperature (RT), samples were further incubated with 2% Triton X-100 (Sigma-Aldrich; 93443) - 0.8% NH_4OH (Sigma-Aldrich; 318612) for 72 h at 4 °C. Lastly, samples were washed with distilled water for 48 h at 4 °C and rinsed three times in PBS at RT. Samples were stored at 4 °C in PBS until further processing.

Protocol n.2 was applied as described by Wolf *et al*. (20). Briefly, after lyophilization (Analis; Alpha 1-4 LDplus), samples were subjected to lipid extraction by incubation for 2 h in 2:1 (v/v) solution of chloroform/methanol at 4 °C. Next, samples were rehydrated using a degrading series of ethanol (100, 90, 70, 50 and 0%) for 30 min each at 4 °C. After this rehydration, samples were subjected for 2 h at 37 °C to an enzymatic treatment with 0.2% Trypsin/0.2% EDTA to remove cellular materials. Then, a chemical treatment with 2% SDC (Sigma-Aldrich; D6750) for 5 h, fresh 2% SDC for 16 h, 1% Triton-X 100 for 1 h, and finally 0.1% (w/v) peracetic acid/4% (v/v) ethanol was perfomed, all at 4 °C. Between each incubation step, samples were once washed with distilled water and twice with PBS for 30 min each, all performed at 4 °C. Samples were stored at 4 °C in PBS until further processing.

Protocol n.3 was applied as described by De Coppi *et al*. (9). Briefly, samples were first rinsed four times with PBS at RT. Next, an incubation step of 72 h in distilled water at 4 °C was followed by 4% SDC for 4 h at 4 °C and 2000 Kunitz units/l DNAse I (Goldbio; D-300-1) in 1M NaCl for 3 h at 37 °C. These incubation steps were repeated once after which the samples were stored in PBS at 4 °C.

Protocol n.4 was applied as described by Ungerleider *et al*. (21). Briefly, samples were first rinsed with distilled water for 30 min at RT. Next, samples were incubated in 1% SDS (Carl Roth; CN30.3) for 2 h after which they were shortly rinsed again, all performed at RT. The samples were subsequently incubated in 1% SDS for 3 days at RT, with short rinses and solution changes every 24 h. After incubation in isopropyl alcohol for 24 h at RT, the samples were transferred to distilled water for 30 min at RT. Next, samples were incubated for another 24 h in fresh distilled water at RT. At the end of the protocol, samples were thoroughly shaken for 30 s to remove air bubbles. Samples were stored at 4 °C in distilled water until further processing.

The in-house protocol was based on the method described by Roosens *et al*. (22) and Philips *et al*. (23). Briefly, samples were first incubated overnight in 50 mM Tris buffer (pH 8) at 4 °C, after which they were transferred to 1% Triton X-100 for 24 h at 4 °C. After two short rinses with Hank's Balanced Salt Solution (HBSS; Sigma-Aldrich; H1387) at RT, an enzymatic treatment with 40 000 Kunitz units/l DNase I and 100 mg/l trypsin (Sigma-Aldrich; T9201) in HBSS at 37 °C for two times 3 h followed. Subsequently, samples were placed in 1% Triton X-100 again for 18 h at 4 °C. Finally, samples were extensively washed with HBSS over 4 days at 4 °C. Samples were stored at 4 °C in HBSS until further processing.

2.3 Macroscopic evaluation

After decellularization, samples were first evaluated macroscopically by placing them on a black background. Representative images were taken with a Canon EOS 1300D, from which the length of the samples could be measured. In addition, transverse dimensions were measured assuming a rectangular shape using an optical micrometer (OptoControl 2600, MicroEpsilo, resolution 0.1 μm). From these

Accepted Manuscript

measurements, the equivalent width, defined as the square root of the cross-sectional area, was defined. Dry tissue weight was also determined after 24 h of lyophilization (Analis; Alpha 1-4 LDplus).

2.4 Histological analysis

Samples for histology (n = 2) were fixed in 4% formaldehyde for 24 h at 4 °C, washed extensively with PBS and dehydrated through an increasing alcohol series (70-80-90-100%). Subsequently, samples were embedded in paraffin. To assess the inner core of the samples, each sample was cut in half, and the inner part was positioned facing downward in the paraffin mould. This ensures an evaluation of the innermost regions during subsequent sectioning. Samples were sectioned at a thickness of 5 µm with a microtome (Leica RM2125 RTS). Overall morphology was evaluated with a haematoxylin-eosin (H&E) staining and intra- and extracellular DNA was visualized with a Feulgen staining. In addition, nuclear remnants were fluorescently stained with 4',6-diamidino-2-phenylindole (DAPI) (Invitrogen; P36935). For evaluation of the ECM, the histochemical stainings Martius Scarlet Blue (MSB) and Alcian Blue were performed to visualize collagen and acid proteoglycans, respectively.

To identify the ECM component laminin, an immunohistochemical staining was performed. After rehydration of the sections, an antigen retrieval step was carried out by treatment with citrate buffer (pH 6) for 25 min at 95 °C, followed by 5 min of pepsin (Sigma-Aldrich; P6887; 4 mg/ml 0.1 M HCl) at 37 °C. Next, nonspecific staining was blocked with blocking buffer containing 1% bovine serum albumin (Sigma-Aldrich; 810533) and 0.2% Tween-20 (Acros Organics; 233360010) for 30 min. The primary antibody rabbit anti-laminin (Sigma-Aldrich; L9393; 1:400) was then incubated overnight at 4 °C. As a secondary antibody, goat anti-rabbit coupled to HRP (Dako; P044801-2; 1:200) was used for 30 min. Subsequently, the peroxidase reaction was visualized with Liquid DAB+ Substrate (Dako; K3467). After counterstaining with Mayer's haematoxylin (Sigma-Aldrich; MHS32), slides were dehydrated, cleared and mounted and imaged with the NanoZoomer-SQ (Hamamatsu).

2.5 Scanning electron microscopy

To evaluate the ultrastructure of the native and decellularized muscle, samples (n = 2) were prepared for scanning electron microscopy (SEM). After 24 h fixation at 4 °C with 2.5% glutaraldehyde (Carl Roth; 4157.1) in 0.05 M cacodylate buffer (pH 7.2) (Carl Roth; 5169.1), samples were washed three times with 0.05 M cacodylate buffer (pH 7.2). Next, samples were fast-frozen in liquid nitrogen and fractured to expose the mid region of the samples which was then marked using a tissue marking dye kit (Klinipath). Samples were further dehydrated with increasing alcohol series (50–75–85–96–100% ethanol) and finally, hexamethyldisilazane (Carl Roth; 3840.2) was used to completely dry the samples. Subsequently, samples were mounted on aluminum stubs using carbon tape and coated with a thin layer of approximately 4 nm of platinum using a JEOL auto fine coater (JFC-1300). Images were recorded with a JEOL scanning electron microscope (JSM-IT200).

2.6 Biochemical analysis and gel electrophoresis

The amount of DNA, GAGs and collagen in native and decellularized samples was determined through biochemical analysis (n = 6) and gel electrophoresis (n = 5). After lyophilization, samples were first processed with papain to obtain fully digested tissue. For this, 1 ml of a 0.2 M sodium phosphate buffer (pH 6.4) containing 8 mg/ml sodium acetate, 4 mg/ml EDTA disodium salt, 0.8 mg/ml cysteine-HCl and 5 µl/ml papain (Sigma-Aldrich; P3125) was added to approximately 10 mg of dry tissue. Due to the low dry weight of samples of the Porzionato and Ungerleider group, samples for gel electrophoresis were pooled to reach the 10 mg of dry tissue, resulting in n = 3 for these groups. Following 18 h incubation at 65 °C, the samples were centrifuged for 10 min at 10 000 g. The supernatant was further used for quantitative analysis with the Qubit dsDNA BR Assay Kit (Thermo Fisher Scientific; Q32850), Blyscan Sulfated Glycosaminoglycan Assay Kit (Biocolor; B-1000) or the Hydroxyproline Assay Kit (Chondrex; #6017) according to the manufacturer's recommendations to determine DNA, GAG and collagen content, respectively. For qualitative analysis, the supernatant was further separated on a 1% agarose gel with GelRed® nuclear stain (VWR; 41011) for visualization. Both a 1 kb and 100 bp DNA ladder (Thermo Fisher Scientific; SM0311 and SM0242) were included as references.

2.7 Mechanical testing

For each decellularization group, six samples were tested, except for the Ungerleider group in which only five samples were sufficient in size. Before testing, the transverse dimensions of the samples were first measured using an optical micrometer (OptoControl 2600, MicroEpsilo, resolution 0.1 µm), assuming a rectangular cross-section. The samples were then mounted on an in-house tensile test machine, described elsewhere (24,25). Comparable clamping conditions between the samples were achieved by tightening with a torque wrench at 0.8 Nm. The samples were subjected to monotonic uniaxial tension until failure, at a pace of 3 mm/min. The stretching pace was chosen low and steady in order to limit any unwanted visco-elastic effect. The force was recorded by means of a 5N load cell (Interface SMT S-type, resolution 0.5 mN), and the position was recorded from an

Accepted Manuscript

internal sensor in the motor (frequency 8 Hz, resolution 0.05 mm). The stress was obtained by dividing the recorded force by the measured initial cross-sectional area of the sample, and the stretch ratio by dividing the recorded distance between the clamps by their initial distance. For post-processing, a stress threshold of 15 kPa was applied, to compensate for the variation in initial stiffness between the samples. A 3rd-order Yeoh's hyperelastic material model (26) was then fit to the experimental data for each sample, assuming the incompressibility of the samples and a purely uniaxial stretch. Under these assumptions, the relation between the stress and the stretch ratio can be written as follows:

$$\sigma = 2\left(\lambda^2 - \frac{1}{\lambda}\right)\sum_{i=1}^{3} iC_i\left(\lambda^2 + \frac{2}{\lambda} - 3\right)^{i-1} \text{ (Eq1)}$$

where σ is the Cauchy stress in the direction of interest, C_i the hyperelastic parameters, and λ the stretch ratio. The Young's modulus was then derived from the first model parameter as follows:

$$E = \lim_{\lambda \to 1}\left(\frac{\partial \sigma}{\partial \lambda}\right) = 6C_1 \text{ (Eq2)}$$

where E is the Young's modulus. The 3rd order was chosen for the model as it presented a better fit than the 1st and 2nd ones in the low stretch ratio range, thus improving the reliability of the calculated Young's modulus. Finally, the ultimate stress and the extensibility (ultimate strain) were determined as those of the last recorded point before failure of the sample.

2.8 Cytocompatibility analysis

To evaluate the cytocompatibility of the decellularized matrices, C2C12 cells, which is a myoblast cell line, were used in both 2D and 3D cultures. For the 2D culture, cryosections of 20 µm were prepared and seeded with $2x10^4$ C2C12 cells in 100 µl of culture medium (DMEM Glutamax supplemented with 10% fetal bovine serum and 1% penicillin/streptomycin). After 24 hours, a live/dead assay was performed in fivefold by replacing the culture medium with 1 ml PBS containing 2 µl calcein-AM (Anaspec; 89201; 1 mg/mL) and 2 µL propidium iodide (Sigma-Aldrich; P4170; 1 mg/mL). After 15 min incubation at room temperature, the samples were rinsed with PBS and analyzed with a ZEISS Z1 observer microscope (ZEISS Microscopy, Jena, Thüringen, Germany).

For the 3D culture, samples were cut to fit a 48-well plate using a biopsy puncher. After overnight incubation in culture medium, samples were transferred to a silicone-coated well plate and $1x10^5$ C2C12 cells were seeded on top of the decellularized matrices. Metabolic activity of the cells was evaluated on day 1 and 3 post-seeding with an alamar blue assay. Briefly, culture medium was replaced by a 44 µM resazurin sodium salt solution (Sigma-Aldrich; 199303-1G) in HBSS (Invitrogen; 14025-050). After 90 min of incubation, fluorescence was measured at an excitation wavelength of 560 nm and an emission wavelength of 590 nm with the GloMax®-Multi Detection System (Promega). In addition, a live/dead assay was performed on day 3 by incubating the samples for 1 hour in PBS containing calcein-AM and propidium iodide as described above. After fixation in 4% PFA, samples were cleared with the 3DISCO protocol as described in (27). In short, samples were first dehydrated with increasing concentrations of tetrahydrofuran (50, 70, 80 and 100%) for 30 min each. The final step with 100% tetrahydrofuran was repeated twice, after which clearing with dibenzyl ether was performed. Samples were then imaged with ZEISS Lightsheet 7 (ZEISS Microscopy, Jena, Thüringen, Germany). The obtained z-scans were visualized and analyzed using the Arivis Vision 4D software (version 4.0).

2.9 Statistical analysis

All statistical analyses were carried out using GraphPad Prism software (GraphPad, Version 9.0.0). Outliers were first identified using the ROUT method, after which normality was assessed with a Shapiro-Wilk normality test. Significant differences between groups were determined using a one-way analysis of variance (ANOVA) with post hoc Tukey's for normally distributed data, while a Kruskal-Wallis test followed by post hoc Dunn's was performed for nonparametric data. Normally distributed data are represented in box plots, while violin plots are used for nonparametric data. A value of $p < 0.05$ was considered to be statistically significant.

3. Results

3.1 Macroscopic evaluation

Across the decellularization groups, macroscopic differences could be observed compared to the native skeletal muscle but also intergroup differences were present. In particular, sample color changed from reddish to whitish and this was most obvious for the Porzionato and Ungerleider protocol **(Figure 1a)**. The samples decellularized by the Wolf and De Coppi protocol had an opaque, beige appearance while the samples decellularized by the Ungerleider protocol appeared opaque white. Differently, samples decellularized with the Porzionato and Roosens protocol appear more transparent but with the latter having a less white appearance. Upon decellularization, samples may undergo alterations in size, manifesting as either shrinkage or elongation **(Figure 1b)**. Notably, the Roosens protocol exhibited a prominent elongation, expanding by

Accepted Manuscript

approximately 50% of its original length. In contrast, samples subjected to the Ungerleider protocol displayed a distinct shrinkage during the decellularization process, marking a significant difference from those treated with the Roosens protocol. Overall, all samples except the De Coppi group showed a significant decrease in equivalent width and dry tissue weight compared to the native skeletal muscle. Equivalent width in the Porzionato, Roosens and Ungerleider groups was found to differ significantly from the native skeletal muscle, Wolf group and De Coppi group **(Figure 1c)**. Lastly, tissue changes produced by the Porzionato and Ungerleider protocol resulted in the highest decrease in dry tissue weight, being statistically different from all other decellularization groups and the native skeletal muscle **(Figure 1d)**.

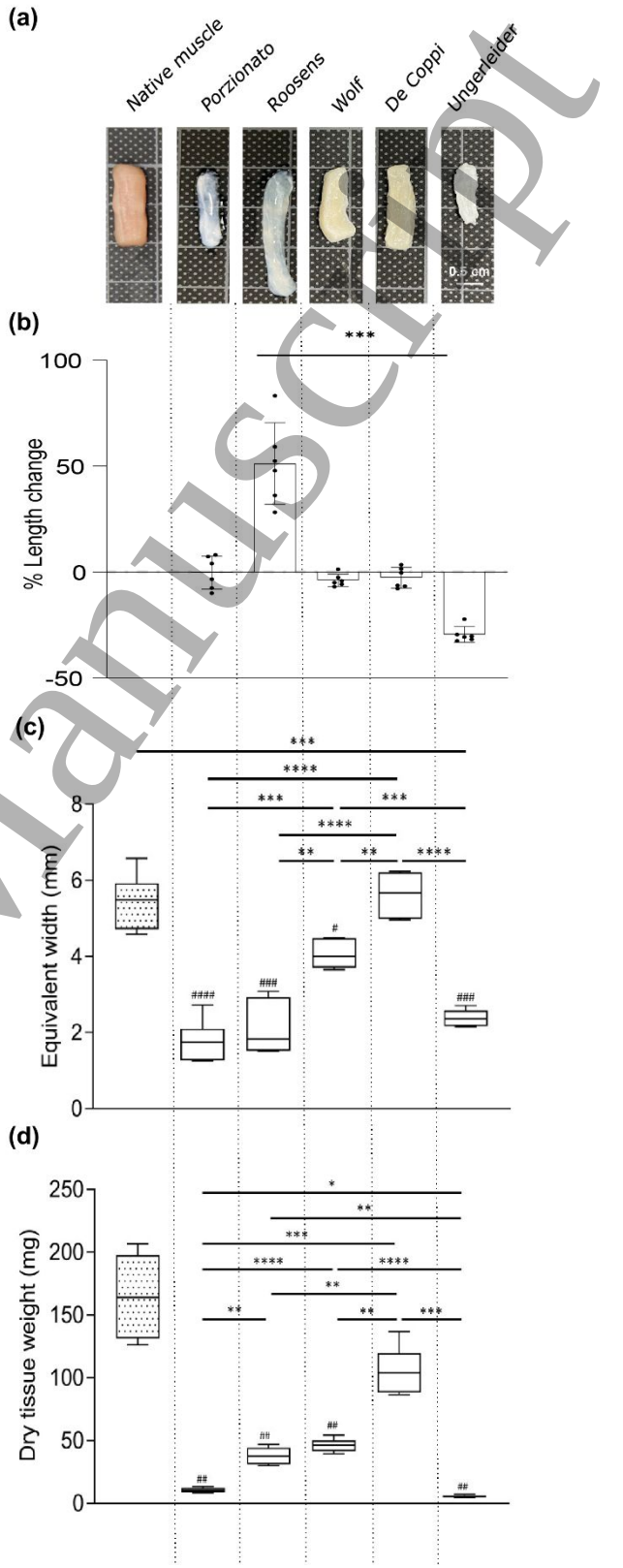

Figure 1. **Macroscopic evaluation of native and skeletal muscle across decellularization groups. (a)** Macroscopic image from each

Accepted Manuscript

decellularization group and native skeletal muscle. **(b)** Percentage length change indicating elongation or shrinkage of the samples after decellularization. **(c)** Sample dimension expressed as equivalent width, defined as the square root of the cross-section, for the various groups. **(d)** Dry tissue weight for the various groups. #$p < 0.05$ compared to native, ##$p < 0.01$ compared to native, ###$p < 0.001$ compared to native, ####$p < 0.0001$ compared to native, *$p < 0.05$ compared to other decellularization groups, ***$p < 0.001$ compared to other decellularization groups, ****$p < 0.0001$ compared to other decellularization groups. (n = 6).

3.2 Histological analysis

To compare the effectiveness of the selected decellularization protocols in removing all nuclear material, a series of specific histological stainings for DNA were performed on longitudinal sections of each group. More specifically, H&E (**Figure 2a)**, Feulgen **(Figure 2b)** and DAPI staining **(Figure 2c)** were used to stain DNA content and nuclei. Intact nuclei across the tissue were still present in the samples decellularized with the De Coppi protocol, while no visible cell nuclei could be detected in the other decellularization groups. However, DNA fragments but no intact nuclei could be observed from the Feulgen and DAPI staining in the Porzionato group despite absence of fragments on the H&E staining. Lastly, on the DAPI staining of samples of the Wolf group, a uniform blue signal can be observed, suggesting autofluorescence of the samples. Beside effective elimination of cells, the aim of decellularization is also to preserve the structure and key proteins of skeletal muscle. To evaluate this, an MSB **(Figure 3a)** and Alcian Blue **(Figure 3b)** histochemical staining were performed on cross-sections to evaluate collagen and GAG content, respectively, along with an immunohistochemical staining for laminin **(Figure 3c)**. The MSB staining demonstrated relative collagen preservation in the endomysium and perimysium in all experimental groups compared to the native condition. The groups in which the cytoplasm content was removed, visible by a loss of red staining, showed an intense blue colour. Similar conclusions could be drawn from the Alcian Blue staining, showing that total GAG content remained relatively unchanged from native muscle tissue. In contrast, laminin was found to be differentially preserved depending on the method used for decellularization. In particular, laminin was almost completely lost in the Porzionato group, while being maintained in the De Coppi and Roosens group. In the Wolf and Ungerleider group, laminin was still present, however, its structural appearance was changed upon decellularization. Finally, overall structure can also be evaluated from the H&E staining performed on the longitudinal sections. Cytoplasm is partially retained by the Roosens, De Coppi and Wolf protocols, while open structures are observed in the Ungerleider and Porzionato group, indicating full removal of the cytoplasm.

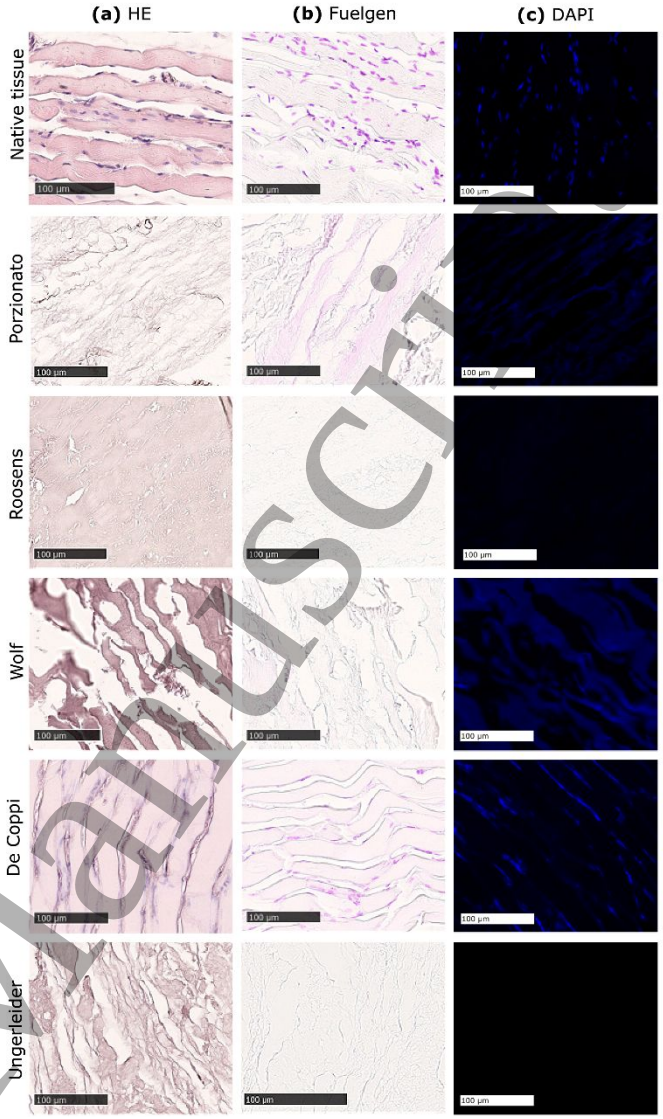

Figure 2. **Histological analysis of the cellular content of native and decellularized skeletal muscle. (a)** H&E staining revealed the presence of remnants of cell nuclei in samples of the De Coppi group, while these were absent in the other decellularization groups. **(b)** DNA remnants were also shown with a Fuelgen staining. This histochemical method demonstrated in pink intact nuclei and DNA remnants in the De Coppi group, while the Porzionato group only contained DNA remnants shown as a spread-out pink smear. **(c)** DNA remnants were also demonstrated with DAPI staining in the De Coppi and Porzionato protocol.

Accepted Manuscript

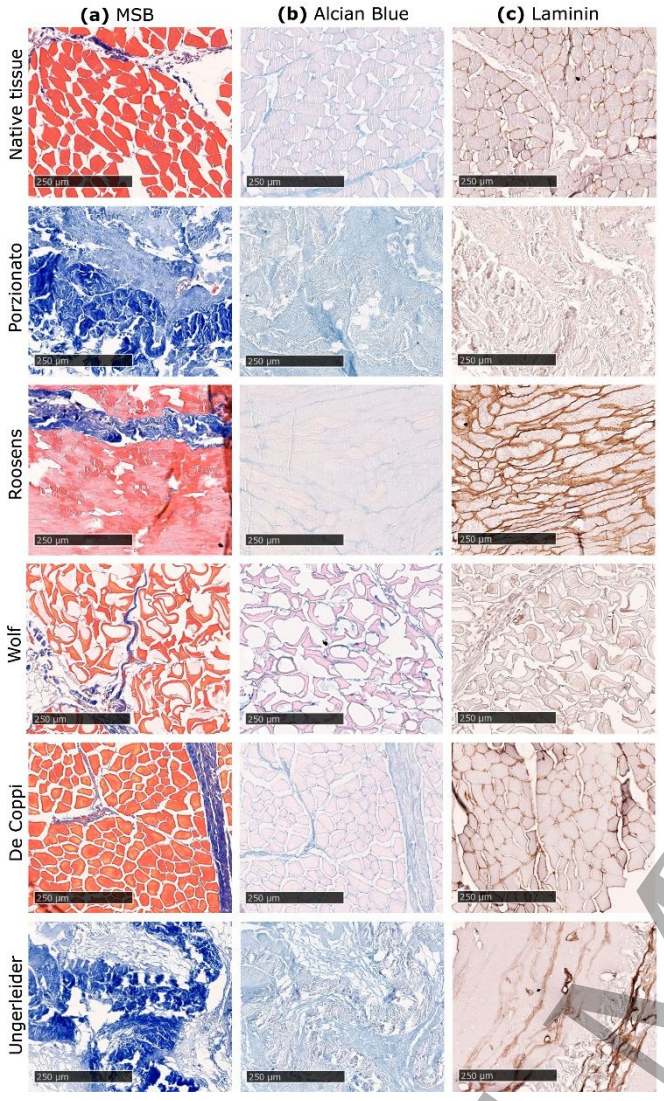

Figure 3. Histological analysis of ECM components of native and decellularized skeletal muscle. (a) Preservation of collagen in all experimental groups was demonstrated by MSB staining. Collagen appears as dark blue, while the cytoplasm stains red. **(b)** Alcian Blue staining showed that acid proteoglycans, visible as light blue, were well preserved in all decellularization groups. The remaining cytoplasm stains light pink. **(c)** Laminin (dark brown) could be found in each group except the Porzionato group as shown with immunohistochemical staining. However, laminin in the skeletal muscle of the Ungerleider and Wolf group did not appear to maintain its original structure and position.

3.3 SEM evaluation of 3D architecture

SEM was used to evaluate if the decellularization process altered the 3D architecture of the decellularized muscle compared to native muscle **(Figure 4)**. Muscle fibers were present in native muscle tissues and the samples decellularized with the De Coppi protocol. In contrast, fibers were found to be removed in the samples decellularized with the Ungerleider protocol leaving hollow and tubular structures. The ECM structure in the samples decellularized with the Roosens and Porzionato protocol showed comparable hollow regions but overall structure appeared less intact. ECM structure of the sample decellularized with the Wolf protocol showed a different appearance, with hollow structures across the whole samples but with a thicker tubule lining.

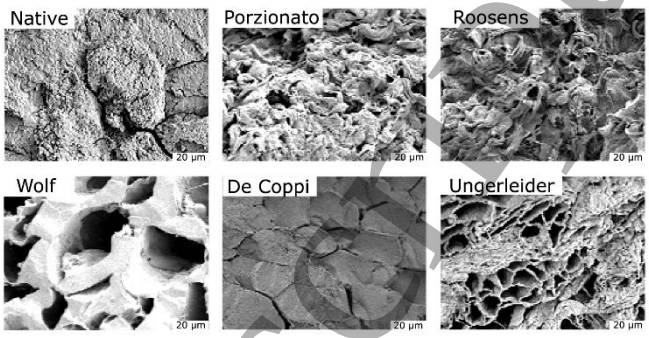

Figure 4: **Ultrastructural analysis of the architecture of native and decellularized skeletal muscle.** Scanning electron microscopic images of cross-sections of native and decellularized skeletal muscle showed preserved tubular, hollow structures in the Ungerleider group. In contrast, muscle fibers were still present in the De Coppi protocol. ECM structure in the Roosens and Porzionato group showed comparable architecture with less intact overall structure. ECM structure of the Wolf group showed hollow structures but with thick tubule lining.

3.4 Biochemical analysis and gel electrophoresis

The extent of decellularization was also quantitatively evaluated through biochemical analysis of DNA, GAG and hydroxyproline (HYP) content, the latter serving as a measure for collagen **(Table 1)**. As for the DNA content, each decellularization protocol resulted in a significant difference compared to native muscle **(Figure 5a)**. Remarkably, upon processing with the Porzionato protocol, a higher ratio of DNA was found compared to the control group, while all other methods resulted in a decrease of nuclear material. More specifically, residual DNA content was approximately 50% for the De Coppi method and was even lower for the other three methods attaining values of 266 ± 44, 345 ± 18 and 270 ± 23 ng/mg for the Roosens, Wolf and Ungerleider method, respectively.

Table 1. Quantitative analysis of DNA, GAG and HYP content of native and decellularized muscle.

	DNA (ng/mg)		GAG (µg/mg)		HYP (µg/mg)	
	Mean	(SEM)	Mean	(SEM)	Mean	(SEM)
Native	1533	(69)	4.86	(0.05)	3.62	(1.66)
Porzionato	3172	(82)	3.97	(0.17)	312.52	(48.25)
Roosens	266	(44)	1.46	(0.08)	25.09	(10.02)
Wolf	345	(18)	2.41	(0.18)	16.46	(0.88)
De Coppi	796	(8)	2.87	(0.09)	9.02	(3.63)
Ungerleider	270	(23)	8.15	(0.52)	504.72	(33.06)

Accepted Manuscript

The GAG content was also significantly affected in each decellularization group, except for the tissue processed with the Porzionato method **(Figure 5b)**. A significantly higher ratio of GAGs was found after processing with the Ungerleider method. In contrast, a significantly lower ratio was found for the Roosens, Wolf and De Coppi protocol. Finally, the HYP content was increased in each of the decellularization groups compared to the native control **(Figure 5c)**. However, this was not statistically different for tissues of the Roosens and De Coppi group. A significant increase was observed for the Porzionato and Ungerleider methods, on the other hand, reaching values of 312.52 ± 48.25 and 504.72 ± 33.06 µg/mg as compared to 3.62 ± 1.66 µg/mg in native tissue.

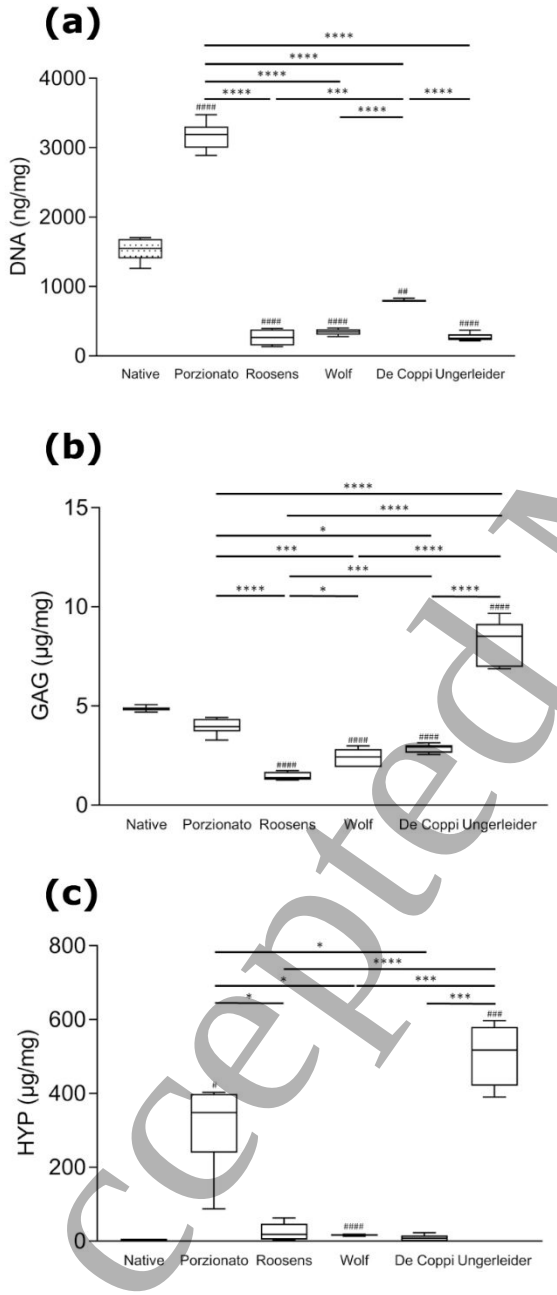

Figure 5. Biochemical analysis of native and decellularized muscle. (a) DNA content is significantly increased in samples of the Porzionato group compared to the native control group, while it is significantly decreased in all other decellularization groups. **(b)** GAG content is significantly decreased in samples of the Roosens, Wolf and De Coppi group, whereas the Ungerleider protocol resulted in a significantly higher value. **(c)** HYP content is increased in all decellularization groups, with significant values for the Porzionato, Wolf and Ungerleider group. #p < 0.05 compared to native, ##p < 0.01 compared to native, ###p < 0.001 compared to native, ####p < 0.0001 compared to native, *p < 0.05 compared to other decellularization groups, ***p < 0.001 compared to other decellularization groups, ****p < 0.0001 compared to other decellularization groups. (n = 6).

Qualitative analysis of DNA content was performed through gel electrophoresis (**Figure 6**). In native tissue, mostly large DNA fragments were found, along with some smaller fragments of less than 250 bp. Samples from the Porzionato group also contained several large DNA fragments, ranging from 1000 to 10 000 bp in length. For the De Coppi group, a wide range of DNA fragments could be observed. Only small DNA fragments of less than 250 bp could be found in the Wolf group, while no apparent DNA fragments were visible for the Roosens and Ungerleider group.

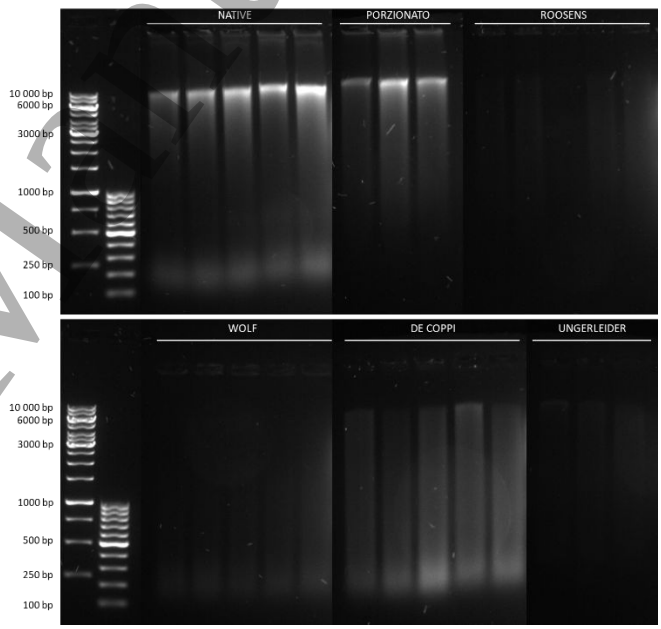

Figure 6. Gel electrophoresis of native and decellularized muscle. Large DNA fragments are visible in the native and Porzionato group. In the De Coppi group, DNA fragments of both large and small size can be observed, while in the Wolf group only small fragments can be found. No apparent DNA fragments were visible in the Roosens and Ungerleider group. (n = 5 for native, Roosens, Wolf and De Coppi; n = 3 for Porzionato and Ungerleider).

3.5 Mechanical testing

Mechanical testing was performed to compare the decellularized samples with native skeletal muscle tissue. Characterization of biomechanical properties is of interest for downstream use of decellularized tissue. For example, for

Accepted Manuscript

implantation, it is desirable that decellularized muscle has similar mechanical properties as compared to the surrounding native muscle. From monotonic uniaxial tensile testing, tissue extensibility, ultimate strength and the Young's modulus could be derived **(Figure 7 and Table 2)**. As for the extensibility, only the Roosens protocol was found to significantly differ from the Wolf, De Coppi and Ungerleider group. Still, none of the decellularized samples differed significantly from the native muscle. The maximum stress the muscle samples could withstand before rupture, indicated by the ultimate strength, was highest in the Roosens and Porzionato group, while the De Coppi, Wolf and Ungerleider groups were close to the native values. However, no significant differences compared to the native group or from the intergroup comparison could be found. Finally, only the elastic modulus of the Roosens group was found to show significant differences as compared to the native muscle and in comparison to the other decellularization groups. Samples of the De Coppi and Ungerleider group were found to be closest related to the native elastic modulus while samples from the Porzionato and Wolf group showed higher variance.

Table 2. Mechanical testing of tissue extensibility, ultimate strength and Young's modulus of native and decellularized muscle.

	Extensibility		Ultimate strength (kPa)		Young's modulus (k	
	Mean	(SEM)	Mean	(SEM)	Median	(Q1 ;
Native	0.58	(0.07)	66.62	(13.98)	45.98	(28.0 60.6
Porzionato	0.54	(0.02)	703.00	(155.2 0)	133.70	(67.6 224.8
Roosens	0.40	(0.04)	441.15	(87.80)	464.90	(386.5 567.5
Wolf	1.11	(0.14)	124.01	(17.67)	114.18	(54.0 160.6
De Coppi	0.74	(0.07)	61.46	(7.98)	55.61	(47.9 65.2
Ungerleider	0.77	(0.05)	168.52	(30.12)	85.04	(70.3 101.9

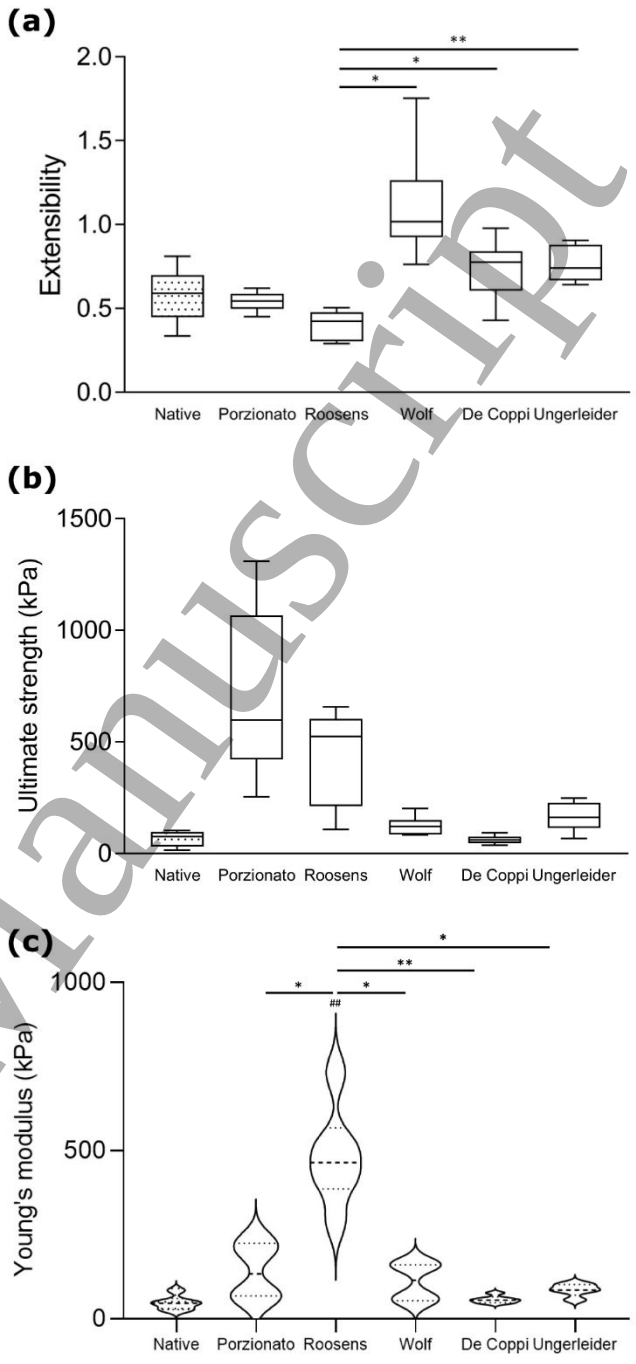

Figure 7. Biomechanical properties of native and decellularized muscle. **(a)** Extensibility is significantly decreased in samples of the Roosens group compared to the Wolf, De Coppi and Ungerleider group. No significant differences across all decellularization groups compared to native skeletal muscle was found. **(b)** Ultimate strength was not found to significantly differ across groups or compared to native skeletal muscle. **(c)** Young's modulus of the Roosens group was found to differ significantly from all decellularization groups and native skeletal muscle. #$p < 0.05$ compared to native, ##$p < 0.01$ compared to native, ###$p < 0.001$ compared to native, ####$p < 0.0001$ compared to native, *$p < 0.05$ compared to other decellularization groups, ***$p < 0.001$ compared to other decellularization groups, ****$p < 0.0001$ compared to other decellularization groups. (n = 6).

Accepted Manuscript

3.6 2D cell attachment on cryosections

To assess the cell attachment to the different decellularized samples, murine myoblasts (C2C12 cells) were seeded on 20 µm thick cryosections. Samples from the De Coppi group were excluded from these (and further 3D) experiments. The decision to exclude the De Coppi protocol while retaining the Porzionato protocol is grounded on the dissimilarity observed in the intactness of nuclei. Specifically, in the Porzionato protocol, nuclei were noted to be fragmented, with no observable intact nuclei evident in both Feulgen and DAPI staining. In contrast, the De Coppi protocol yielded samples with intact nuclei distributed across the tissue (**Figure 2b,c)**.

Cell-ECM attachment was imaged 24 hours after seeding by labeling living cells with calcein-AM followed by visualization of green fluorescence and brightfield **(Figure 8a)**. A significantly lower cell attachment was seen for the cells seeded on the cryosections of the samples decellularized with the Wolf protocol compared to the other three protocols **(Figure 8c)**. Using a propidium iodide staining, the ratio of dead cells versus living cells was determined **(Figure 8b)**. In general, all conditions showed limited cell death with some sparse regions containing clusters of dead cells in the Roosens protocol, however not significantly different from the other conditions **(Figure 8d)**. On the other hand, a significant difference was found between the Porzionato and Ungerleider protocols, showing a significantly lower incidence of cell death among the cells seeded on cryosections obtained through the former.

3.7 Cell attachment on 3D decellularized muscle

Cell attachment was assessed by seeding $1x10^5$ C2C12 cells on decellularized samples (dimensions: see Figure 1). Cell attachment and infiltration were evaluated after three days and visualized using lightsheet microscopy **(Figure 9a)**. The decellularized samples obtained through the Ungerleider protocol exhibited the highest total volume of attached myoblasts **(Figure 9c)**, with the median volume of the individual myoblasts also being significantly higher compared to all other conditions **(Figure 9b)**. Moreover, the volume of individual myoblasts attached to the decellularized samples was significantly different across all groups **(Figure 9b)**.

In addition to volumetric assessments, the morphological characteristics of attached cells were investigated by quantifying cell sphericity **(Figure 9c)**. Notably, median cell sphericity exhibited significant differences across all decellularization protocols. The Roosens protocols yielded the highest mean sphericity, suggesting a prevalence of round-shaped cells. Conversely, the Ungerleider protocol produced the lowest mean sphericity, indicating a prevalence of more elongated cells.

Additionally, cell metabolism was assessed using an alamar blue assay at day 3 relative to day 1 after seeding. Most cells were observed in the Porzionato and Ungerleider samples, showing an elongated morphology. Fewer cells were observed to be attached on the Roosens and Wolf samples and cells were found with a more round morphology. With the metabolic assay it was observed that cell metabolism remained constant for the Porzionato samples whereas it was significantly increased in the Ungerleider samples. In addition, 3D movies of the acquired z-stacks show the cells mainly at the surface of the samples after three days of incubation **(Supplementary videos 1-4)**.

3.8 General impact of decellularization methods

To summarize the main effects of the different decellularization protocols, an overview is given in **Table 3**. Overall, the Porzionato protocol resulted in an inefficient removal of DNA content although cytoplasmic proteins were completely removed. In addition, collagen and GAGs were well preserved, but laminin was no longer present and stiffness of the samples was increased compared to the native control group. Cell attachment was good, both in 2D and 3D, but no increase in metabolic activity was noted over time. On the other hand, DNA content in samples of the Roosens group was drastically decreased, with no more visible DNA fragments, along with preservation of collagen and laminin, but with a significant decrease of GAGs and significant increase of stiffness. The cytocompatibility analysis also revealed some areas with more dead cells, however, overall cell attachment was good and a slight increase of metabolic activity could be observed. Decellularization with the Wolf method also resulted in a significant decrease of DNA content and the appearance of hollow tubular structures, although cytoplasm was not removed. Furthermore, a significant decrease of GAG content was observed, but collagen and laminin were preserved. Stiffness of the samples was increased as well, but not in a significant manner. Interestingly, cell attachment on these samples was significantly lower compared to the other groups. The protocol according to De Coppi only resulted in a 52% decrease of DNA content with large DNA fragments remaining and limited removal of cytoplasm. Therefore, these samples were excluded from the cytocompatibility analysis. Collagen and laminin were preserved, but GAG content was significantly decreased. The biomechanical properties, however, were similar to native muscle. Finally, processing with the Ungerleider method resulted in a significant decrease of DNA content without visible DNA fragments along with removal of the cytoplasm, creating hollow tubular structures. Collagen, GAGs and laminin were preserved and

Accepted Manuscript

biomechanical properties remained similar to native skeletal muscle. Moreover, a good cell attachment was observed in 2D and 3D, and metabolic activity was the highest after three days.

Accepted Manuscript

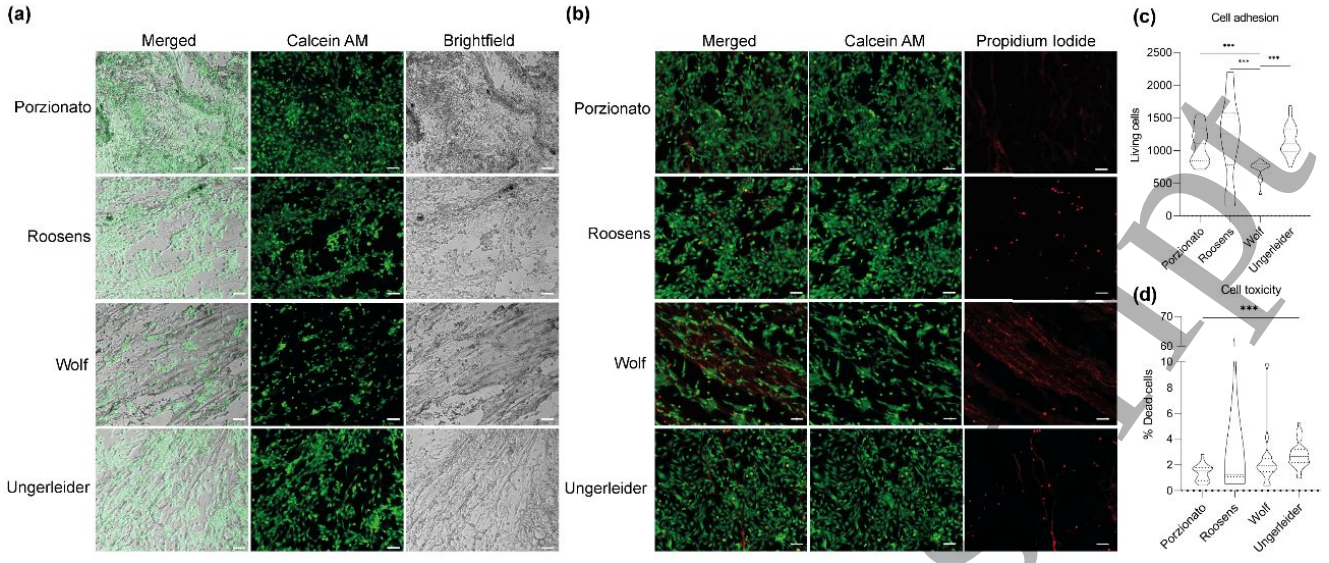

Figure 8. Cell attachment on 20 µm thick cryosections of decellularized skeletal muscle samples. (a) Representative brightfield images combined with green fluorescent images to show cell attachment (green, calcein-AM) after 24 hours to the ECM of decellularized skeletal muscle obtained using the various protocols. Scale bar represents 100 µm. **(b)** Representative images of the live/dead assay performed 24 hours after seeding the cells on the ECM of decellularized skeletal muscle obtained using the various protocols showing living cells (green, calcein-AM) and dead cells (propidium iodide, red). Scale bar represents 100 µm. Autofluorescence of the ECM matrix can be seen in the red channel. **(c)** Number of cells attached to the ECM of the different protocols. A significantly lower amount of cells was found to attach to the sections of the ECM obtained using the Wolf protocol. **p < 0.01 compared to other decellularization groups, ***p < 0.001 compared to other decellularization groups. Quantifications based on n = 20 pictures obtained from sections of 2 different biological replicates. n = 17 for the Wolf conditions due to higher detachment of the sections upon cell seeding. Values are normalized to the size of one microscopic image. **(d)** Percentage of dead cells in comparison to the total amount of attached cells. A significant difference was found between the Porzionato and Ungerleider protocols, showing a significantly lower incidence of cell death among the cells seeded on cryosections obtained through the former. Quantifications based on n = 20 pictures obtained from sections of 2 different biological replicates. n = 17 for the Wolf conditions due to higher detachment of the sections upon cell seeding.

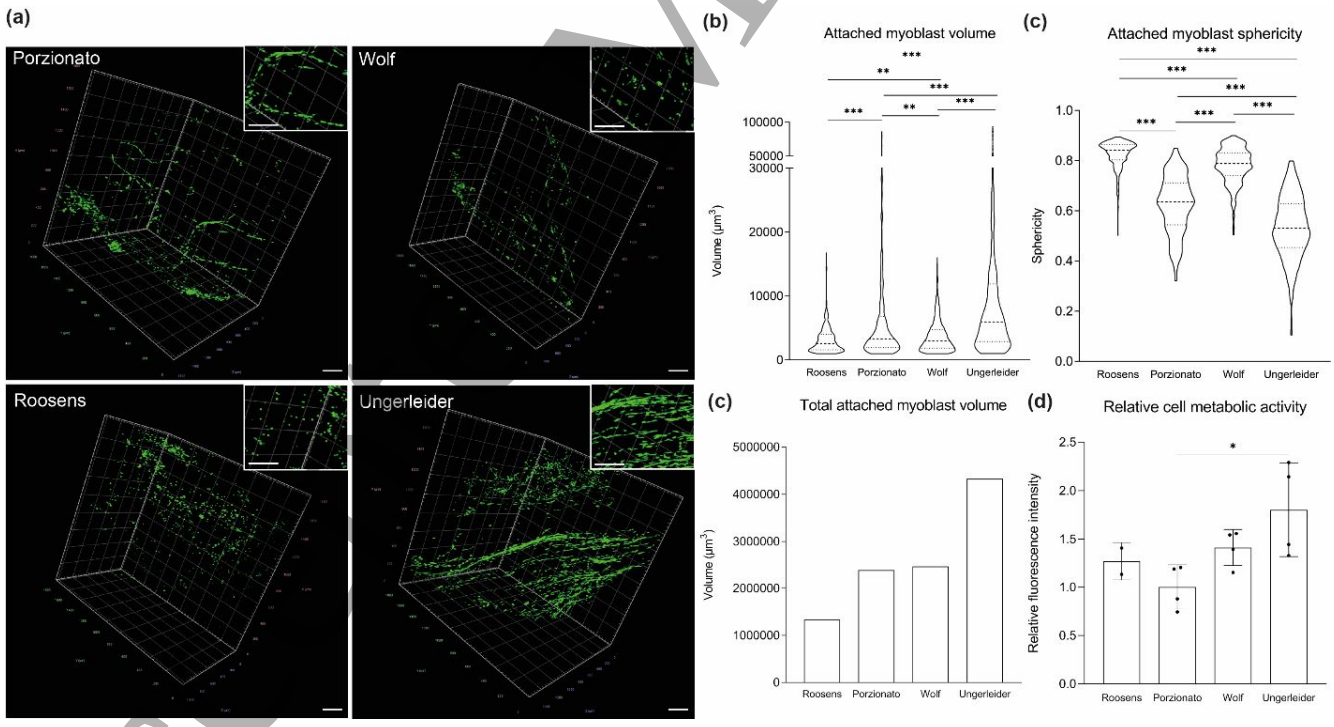

Figure 9. Cell attachment to 3D decellularized skeletal muscle samples. (a) Representative 3D reconstruction of a z-stack generated with a lightsheet microscope of cleared 3D decellularized samples seeded with $1x10^5$ C2C12 cells (calcein-AM, green). Inset in the right corner shows a magnified region to visualize cell morphology. Scale bars represent 200 µm. Images were acquired of at least 4 biological replicates per group. **(b)** Graphical representation of the

volume of individual myoblasts attached to the decellularized samples found throughout the entire z-scan. **p < 0.01 compared to other decellularization groups. ***p < 0.001 compared to other decellularization groups. **(c)** Graphical representation of the total volume of attached myoblasts seeded on the 3D decellularized samples. **(d)** Graphical representation of the sphericity of the individual attached myoblasts seeded on the 3D decellularized samples. ***p < 0.001 compared to other decellularization groups. **(b-d)** Quantifications on the 3D decellularized samples were performed on 1 representative sample of each condition, entirely scanned using lightsheet microscopy (n = 1). **(e)** Relative metabolic cell activity of myoblasts on day 3 after seeding compared to day 1. A significant increase in cell metabolism was found for the Ungerleider condition compared to the Porzionato condition. *p < 0.05 compared to other decellularization groups. (n = 2 for the Roosens group, n = 4 for the other groups).

Accepted Manuscript

Table 3. Overview of the impact of the different decellularization protocols.

	Evaluation	Native	Porzionato	Roosens	Wolf	De Coppi	Ungerleider
Macroscopic appearance	Tissue dry weight (mg)	164.78 ± 36.75	10.57 ± 1.99	37.90 ± 7.08	46.28 ± 5.48	105.67 ± 19.11	5.77 ± 0.85
Cellular content							
Nuclear remnants	Histology	+++	++	-	-	+++	-
	Biochemistry (ng/mg)	1533 ± 69	3172 ± 82	266 ± 44	345 ± 18	796 ± 8	270 ± 23
	Gel electrophoresis	Small and large DNA fragments	Large DNA fragments	No DNA fragments	Small DNA fragments	Small and large DNA fragments	No DNA fragments
Cytoplasmic remnants	Histology	+++	-	+++	++	+++	-
	SEM		Complete removal	Partial removal	Partial removal	No removal	Complete removal
ECM composition							
Collagen	Histology	++	+++	++	++	++	+++
	Biochemistry (µg/mg)	3.62 ± 0.74	312.52 ± 48.25	25.09 ± 10.02	16.46 ± 0.88	9.02 ± 3.63	504.72 ± 33.06
GAGs	Histology	++	+++	+	+	++	+++
	Biochemistry (µg/mg)	4.86 ± 0.05	3.97 ± 0.17	1.46 ± 0.08	2.41 ± 0.44	2.87 ± 0.09	8.15 ± 0.52
Laminin	Histology	++	-	+++	+	++	++
Mechanical integrity	Tensile test		Increased stiffness	Significantly increased stiffness	Increased stiffness	Similar to native muscle	Similar to native muscle
Cytocompatibility							
2D attachment	Live/dead assay	ND	Good	Good, some dead cells	Lower attachment	ND	Good
3D attachment	Live/dead assay	ND	Elongated cells	Round cells	Round cells	ND	Elongated cells
Metabolic activity	Alamar blue assay	ND	No increase	Slight increase	Slight increase	ND	Significant increase

Histological reactions were scored as absent (-), weak reaction (+), moderate reaction (++) or strong reaction (+++). ND = not determined.

Accepted Manuscript

4. Discussion

Decellularized skeletal muscle is emerging as an attractive treatment option for VML injuries. However, a major challenge is to translate successful results in rodents to larger animal models, partially due to the differences in dimensions of the tissue. In the present study, our goal was to compare a newly developed decellularization protocol to four previously published methods in a standardized manner. The use of an extensive set of evaluation methods allows for a more thorough understanding of the impact of different decellularizing agents on the structure and composition of skeletal muscle, which is now often lacking. Moreover, some of the previous protocols have only been applied to thin muscle sections. By using porcine tissues with a thickness of 5 mm we reach sample dimensions with an increased clinical relevance and enable a comparison across the different protocols.

The first aspect that was thoroughly analyzed was the efficiency of the decellularization protocols to remove the nuclear content. From both the histological analysis, including H&E, Feulgen and DAPI staining as well as the quantitative and qualitative analysis of DNA content, it was clear that the method according to De Coppi *et al*. (9) which consisted of two cycles of SDC and DNase I treatment did not result in effective removal of DNA from our samples. Similar results have been observed by Naik *et al*. for the decellularization of human zygomaticus muscle, even after four cycles of SDC and DNase I (11). On the other hand, when employing the Porzionato method, muscle tissue samples appeared cell-free based on the H&E staining, but nuclear remnants were revealed with DAPI and Feulgen staining, and large DNA fragments were still visible with gel electrophoresis. Surprisingly, DNA quantification even resulted in a higher DNA content compared to native tissue. This is due to expressing DNA content relative to dry tissue weight. An equal amount of total DNA will result in a higher ratio if lipids, proteins or other components contributing to tissue weight have been removed due to decellularization. Indeed, samples from the Porzionato group appeared more transparent and had a significantly lower dry tissue weight upon decellularization, suggesting removal of a large part of the samples. In combination with a minor impact on DNA, this ultimately resulted in an increased ratio of DNA content. In contrast, tissues processed according to the Roosens, Wolf or Ungerleider method resulted in a drastic decrease of DNA content. For the Wolf group, however, a uniform blue signal was noted on DAPI staining. This might be due to autofluorescene of the samples after treatment with Triton X-100 (28). The short rinse with PBS at the end of this method might not have been sufficient to entirely wash away residual detergent, resulting in a strong fluorescent signal. In addition, the criterion of Crapo *et al*. (29) stating that only 50 ng dsDNA per mg ECM dry weight may remain was not fulfilled for either of the three best-performing methods. In this context it is important to mention that the original protocol developed by Wolf *et al*. was evaluated on muscle sheets of only 2.25 mm thickness (20). Similarly, the Roosens protocol was initially developed for decellularization of porcine heart valves and later on for rat peripheral nerves (22,23). Both of these tissues have a limited thickness, emphasizing again the challenges to obtain fully decellularized skeletal muscle tissue with increased thickness. Nevertheless, the DNA criteria as originally described by Crapo *et al*. (29) might be too stringent and may need a revision based on progress made in the field. Indeed, some ECM-based materials that are already in use in the clinic, such as urinary bladder matrix (Matristem®, ACell) and small intestinal submucosa (Biodesign®, Cook Biotech), were found to have levels above the set criterion reaching values of even 2 µg/mg ECM dry weight (30).

In addition to eliminating all nuclear content, it could be hypothesized that removal of the cytoplasm of the myofibers is beneficial as well. In this way, only the ECM will remain, allowing host satellite cells to migrate through the hollow tubes upon transplantation. It has been demonstrated before that the presence of cytoplasmic proteins in decellularized tissues creates a mechanical obstacle for satellite cells during regeneration and ultimately results in myofibers of inferior quality (31). MSB staining revealed that only processing with the Porzionato and Ungerleider protocol resulted in complete removal of cytoplasm. The former method, however, also resulted in complete removal of laminin as demonstrated with immunohistochemistry, along with a distorted appearance of the remaining ECM as seen with SEM. This indicates that applying 2% Triton X-100 for 72 h might be a too harsh method for decellularization of skeletal muscle. When decreasing the concentration to 1% and limiting the exposure time as included in the Roosens protocol, excellent preservation of laminin is seen. However, with this milder decellularization protocol, not all cytoplasm is removed from the muscle samples. Protocols including the detergent SDC are not capable of achieving this removal either, since a clear red color is still visible with MSB staining for samples processed with the Wolf and De Coppi protocol. These results are consistent with previous studies conducted on mice diaphragm and the lower limb of rats (31,32). It appears that only the detergent SDS is suitable to remove cytoplasmic proteins without significantly altering the ECM as demonstrated before for other dense tissues such as tendon (33,34). Interestingly, even higher GAG and HYP ratios compared to native tissue were observed with this protocol. This can again be explained by the expression of GAG and HYP content relative to tissue dry weight.

To further evaluate the impact of the decellularizing agents on the tissue ultrastructure, SEM was included in this study. Each

Accepted Manuscript

decellularization protocol clearly had a different impact, confirming the histological analysis. Samples processed with the De Coppi protocol most closely resembled native tissue as expected. In contrast, after processing with the Wolf or Ungerleider protocol, hollow tubular structures could be observed. Interestingly, the diameter of these structures and the thickness of the wall seems to differ. Based on the MSB staining, it appears that in samples of the Wolf group, the cytoplasm has been displaced and contributes to the wall of the tubular structure in addition to the ECM components. This might be due to the lyophilization step which is included in the Wolf method leading to formation of ice crystals inside the tissue and subsequently resulting in an open structure. The tubular structures in samples of the Ungerleider group are alternated with regions displaying loss of structural organization. This is also observed in the MSB staining which shows dense collagen regions. The exposure to the detergent SDS might have been too extensive, resulting in precipitation of proteins such as collagen, as described previously (29). For future studies, it might also be interesting to take a closer look at the impact on the ultrastructure of blood vessels and nerves embedded within the ECM. This becomes particularly pertinent when scaling up to larger tissues, where preserving these structures becomes vital. Ensuring the integrity of blood vessels and nerves is crucial for sustaining adequate oxygen and nutrient supply, as well as facilitating proper innervation after the transplantation of decellularized matrices into the host and during subsequent regenerative processes.

Based on histological and biochemical analysis, the ECM composition was generally well-preserved after each of the decellularization methods, with the exception of the Porzionato method which resulted in complete loss of laminin. In addition, both the Roosens and Wolf method resulted in a significant decrease of GAGs. These minor alterations seem to influence the biomechanical properties of the tissues, since the highest variations in ultimate strength and Young's modulus were seen for samples of these three groups. The common use of Triton X-100 and trypsin in each of these methods might be the underlying reason for altered biomechanical properties, as has been observed in the original study of Porzionato *et al*. as well (10). However, caution should be taken when interpreting these results, as it is difficult to accurately measure the cross-sectional area of the tissue after decellularization to allow for calculation of the mentioned parameters. Soft tissues tend to deform under the influence of gravity, reducing the accuracy of thickness measurements.

Finally, cytocompatibility experiments were carried out to evaluate cellular interaction with the decellularized matrices. From the 2D assay, possible cytotoxicity could be detected due to the direct exposure of the cells to the inner part of the matrix. Interestingly, in samples of the Roosens group, several regions displayed clusters of dead cells. This might be due to remaining detergents or enzymes and poses a hurdle for future *in vivo* use. For the other groups, almost no dead cells were observed, indicating that the final washing steps properly removed the decellularizing agents. As for cell attachment, it was noted that fewer cells adhered to samples of the Wolf group, both in 2D and 3D. This could be caused by the significant amount of cytoplasm that is still present after this decellularization protocol. As pointed out above, it has previously been shown that the remaining cytoplasm hinders skeletal muscle regeneration (31). For samples of the Porzionato and Ungerleider group, the initial attachment in 3D was similar. However, after three days of culture, no increase in metabolic activity was seen in the former group. Furthermore, a difference in cell morphology was observed, where cells in the Ungerleider group showed a more elongated morphology. This is consistent with the ultrastructural data where honeycomb-like pores could be observed similar to the connective tissue organization of the native muscle and in which new cells could better attach and elongate. Cell alignment is an important feature for myotube organization and muscle regeneration.

5. Conclusion

Based on our observations, we could conclude that the De Coppi method using 4% SDC in combination with DNase I is not an effective method for decellularization of thicker skeletal muscle tissue. Triton X-100 in combination with trypsin, on the other hand, is able to remove nuclear material but not cytoplasmic proteins at low concentrations. Moreover, it could lead to significant alterations of the biomechanical properties of the tissue and seems to be difficult to wash away from the matrix, resulting in cytotoxicity. Finally, the Ungerleider method using 1% SDS seems most promising for immersion decellularization of skeletal muscle tissue with dimensions of 20 x 5 x 5 mm, although further finetuning might still be possible. Future research on immersion decellularization might explore the use of lower concentrations, alternative combinations of decellularizing agents and varying incubation times. For larger and/or more complex samples such as full limbs, perfusion decellularization, which makes use of the existing vasculature, is likely to improve the penetration of decellularizing agents deep into the tissue. Either way, an appropriate set of evaluation methods, as described in the present study, will be crucial to determine the impact of future decellularization protocols on the nuclear content, the resulting matrix and cellular interaction.

Acknowledgements

The authors are grateful to Jean-François Witz for assistance with mechanical tests, to Linda Desender for assistance with

Accepted Manuscript

histology and to Sigrid Vanryckeghem for administrative support. This work was funded by Fonds Wetenschappelijk Onderzoek – Vlaanderen (1133520N mandate to Lisanne Terrie and project G0D3620N) and I-SITE joint doctorate ISPLI/18/036.

Data availability statement

The datasets supporting the conclusions of this article are available in the Open Science Framework repository (https://osf.io/vcn38/). The raw data are available from the corresponding author on reasonable request.

Conflict of interest

Not applicable.

References

1. Mukund K, Subramaniam S. Skeletal muscle: A review of molecular structure and function, in health and disease. Wiley Interdiscip Rev Syst Biol Med [Internet]. 2020 Jan 13;12(1):e1462. Available from: https://onlinelibrary.wiley.com/doi/abs/10.1002/wsbm.1462
2. Corona BT, Wenke JC, Ward CL. Pathophysiology of Volumetric Muscle Loss Injury. Cells Tissues Organs [Internet]. 2016;202(3–4):180–8. Available from: https://www.karger.com/Article/FullText/443925
3. Agostini T, Lazzeri D, Spinelli G. Anterolateral thigh flap: Systematic literature review of specific donor-site complications and their management. J Cranio-Maxillofacial Surg [Internet]. 2013;41(1):15–21. Available from: http://dx.doi.org/10.1016/j.jcms.2012.05.003
4. Qazi TH, Mooney DJ, Pumberger M, Geißler S, Duda GN. Biomaterials based strategies for skeletal muscle tissue engineering: Existing technologies and future trends. Biomaterials [Internet]. 2015 [cited 2017 Sep 15];53:502–21. Available from: http://ac.els-cdn.com/S0142961215002483/1-s2.0-S0142961215002483-main.pdf?_tid=ab655ebe-9a0d-11e7-918e-00000aab0f6b&acdnat=1505477097_dd0d4918de1a7410a83ae067b4417aab
5. Zhang W, Liu Y, Zhang H. Extracellular matrix: an important regulator of cell functions and skeletal muscle development. Cell Biosci [Internet]. 2021;11(1):1–13. Available from: https://doi.org/10.1186/s13578-021-00579-4
6. Li EW, McKee-Muir OC, Gilbert PM. Cellular Biomechanics in Skeletal Muscle Regeneration. In: Current Topics in Developmental Biology [Internet]. 1st ed. 2018. p. 125–76. Available from: http://dx.doi.org/10.1016/bs.ctdb.2017.08.007
7. Gamba PG, Conconi MT, Lo Piccolo R, Zara G, Spinazzi R, Parnigotto PP. Experimental abdominal wall defect repaired with acellular matrix. Pediatr Surg Int [Internet]. 2002 Sep;18(5–6):327–31. Available from: http://www.ncbi.nlm.nih.gov/pubmed/12415348
8. Conconi MT, Coppi P De, Bellini S, Zara G, Sabatti M, Marzaro M, et al. Homologous muscle acellular matrix seeded with autologous myoblasts as a tissue-engineering approach to abdominal wall-defect repair. Biomaterials [Internet]. 2005 May;26(15):2567–74. Available from: https://linkinghub.elsevier.com/retrieve/pii/S0142961204006878
9. De Coppi P, Bellini S, Conconi MT, Sabatti M, Simonato E, Gamba PG, et al. Myoblast-acellular skeletal muscle matrix constructs guarantee a long-term repair of experimental full-thickness abdominal wall defects. Tissue Eng [Internet]. 2006/08/08. 2006 Jul;12(7):1929–36. Available from: https://www.liebertpub.com/doi/10.1089/ten.2006.12.1929
10. Porzionato A, Sfriso M, Pontini A, Macchi V, Petrelli L, Pavan P, et al. Decellularized Human Skeletal Muscle as Biologic Scaffold for Reconstructive Surgery. Int J Mol Sci [Internet]. 2015 Jul 1;16(12):14808–31. Available from: http://www.mdpi.com/1422-0067/16/7/14808
11. Naik A, Griffin MF, Szarko M, Butler PE. Optimizing the decellularization process of human maxillofacial muscles for facial reconstruction using a detergent-only approach. J Tissue Eng Regen Med [Internet]. 2019 Sep 25;13(9):1571–80. Available from: https://onlinelibrary.wiley.com/doi/10.1002/term.2910
12. Fishman JM, Ansari T, Sibbons P, De Coppi P, Birchall MA. Decellularized Rabbit Cricoarytenoid Dorsalis Muscle for Laryngeal Regeneration. Ann Otol Rhinol Laryngol [Internet]. 2012 Feb 1;121(2):129–38. Available from: http://journals.sagepub.com/doi/10.1177/000348941212100210
13. Perniconi B, Costa A, Aulino P, Teodori L, Adamo S, Coletti D. The pro-myogenic environment provided by whole organ scale acellular scaffolds from skeletal muscle. Biomaterials. 2011;32(31):7870–82.
14. Wassenaar JW, Boss GR, Christman KL. Decellularized skeletal muscle as an in vitro model for studying drug-extracellular matrix interactions. Biomaterials. 2015 Sep;64:108–14.
15. DeQuach JA, Mezzano V, Miglani A, Lange S, Keller GM, Sheikh F, et al. Simple and high yielding method for preparing tissue specific extracellular matrix coatings for cell culture. PLoS One. 2010;5(9):1–11.
16. Stern MM, Myers RL, Hammam N, Stern KA, Eberli D, Kritchevsky SB, et al. The influence of extracellular matrix derived from skeletal muscle tissue on the proliferation and differentiation of myogenic progenitor cells ex vivo. Biomaterials. 2009;30(12):2393–9.
17. Chen XK, Walters TJ. Muscle-derived decellularised extracellular matrix improves functional recovery in a rat latissimus dorsi muscle defect model. J Plast Reconstr Aesthetic Surg. 2013;66(12):1750–8.
18. Corona BT, Wu X, Ward CL, McDaniel JS, Rathbone CR, Walters TJ. The promotion of a functional fibrosis in skeletal muscle with volumetric muscle loss injury following the transplantation of muscle-ECM. Biomaterials. 2013;34(13):3324–35.
19. Wang L, Johnson JA, Chang DW, Zhang Q. Decellularized musculofascial extracellular matrix for tissue engineering. Biomaterials. 2013 Apr;34(11):2641–54.
20. Wolf MT, Daly KA, Reing JE, Badylak SF. Biologic scaffold composed of skeletal muscle extracellular matrix. Biomaterials [Internet]. 2012/01/24. 2012 Apr;33(10):2916–25. Available from: https://linkinghub.elsevier.com/retrieve/pii/S0142961212000087

Accepted Manuscript

21. Ungerleider JL, Johnson TD, Rao N, Christman KL. Fabrication and characterization of injectable hydrogels derived from decellularized skeletal and cardiac muscle. Methods [Internet]. 2015 Aug;84:53–9. Available from: https://linkinghub.elsevier.com/retrieve/pii/S1046202315001413
22. Roosens A, Somers P, De Somer F, Carriel V, Van Nooten G, Cornelissen R. Impact of Detergent-Based Decellularization Methods on Porcine Tissues for Heart Valve Engineering. Ann Biomed Eng [Internet]. 2016 Sep 2 [cited 2018 Jan 24];44(9):2827–39. Available from: http://link.springer.com/10.1007/s10439-016-1555-0
23. Philips C, Campos F, Roosens A, Sánchez-Quevedo M del C, Declercq H, Carriel V. Qualitative and Quantitative Evaluation of a Novel Detergent-Based Method for Decellularization of Peripheral Nerves. Ann Biomed Eng [Internet]. 2018 Nov 9;46(11):1921–37. Available from: http://link.springer.com/10.1007/s10439-018-2082-y
24. Morch A, Pouseele B, Doucède G, Witz J-F, Lesaffre F, Lecomte-Grosbras P, et al. Experimental study of the mechanical behavior of an explanted mesh: The influence of healing. J Mech Behav Biomed Mater [Internet]. 2017 Jan;65:190–9. Available from: https://linkinghub.elsevier.com/retrieve/pii/S1751616116302491
25. Astruc L, De Meulaere M, Witz J-F, Nováček V, Turquier F, Hoc T, et al. Characterization of the anisotropic mechanical behavior of human abdominal wall connective tissues. J Mech Behav Biomed Mater [Internet]. 2018 Jun;82:45–50. Available from: https://www.sciencedirect.com/science/article/pii/S1751616118302959
26. Yeoh OH. Some Forms of the Strain Energy Function for Rubber. Rubber Chem Technol [Internet]. 1993 Nov 1;66(5):754–71. Available from: https://doi.org/10.5254/1.3538343
27. Decroix L, Van Muylder V, Desender L, Sampaolesi M, Thorrez L. Tissue clearing for confocal imaging of native and bio-artificial skeletal muscle. Biotech Histochem [Internet]. 2015 Apr 20 [cited 2015 Jun 1];90(6):424–31. Available from: http://dx.doi.org/10.3109/10520295.2015.1019564
28. Piña R, Santos-Díaz AI, Orta-Salazar E, Aguilar-Vazquez AR, Mantellero CA, Acosta-Galeana I, et al. Ten Approaches That Improve Immunostaining: A Review of the Latest Advances for the Optimization of Immunofluorescence. Int J Mol Sci [Internet]. 2022 Jan 26;23(3):1426. Available from: https://www.mdpi.com/1422-0067/23/3/1426
29. Crapo PM, Gilbert TW, Badylak SF. An overview of tissue and whole organ decellularization processes. Biomaterials. 2011 Apr;32(12):3233–43.
30. Huleihel L, Hussey GS, Naranjo JD, Zhang L, Dziki JL, Turner NJ, et al. Matrix-bound nanovesicles within ECM bioscaffolds. Sci Adv. 2016;2(6).
31. Urciuolo A, Urbani L, Perin S, Maghsoudlou P, Scottoni F, Gjinovci A, et al. Decellularised skeletal muscles allow functional muscle regeneration by promoting host cell migration. Sci Rep [Internet]. 2018;8(1):8398. Available from: http://www.ncbi.nlm.nih.gov/pubmed/29849047
32. Piccoli M, Urbani L, Alvarez-Fallas ME, Franzin C, Dedja A, Bertin E, et al. Improvement of diaphragmatic performance through orthotopic application of decellularized extracellular matrix patch. Biomaterials [Internet]. 2016 Jan;74:245–55. Available from: https://linkinghub.elsevier.com/retrieve/pii/S0142961215008091
33. Woods T, Gratzer PF. Effectiveness of three extraction techniques in the development of a decellularized bone–anterior cruciate ligament–bone graft. Biomaterials. 2005 Dec 1;26(35):7339–49.
34. Cartmell JS, Dunn MG. Effect of chemical treatments on tendon cellularity and mechanical properties. J Biomed Mater Res [Internet]. 2000 Jan 1;49(1):134–40. Available from: https://doi.org/10.1002/(SICI)1097-4636(200001)49:1%3C134::AID-JBM17%3E3.0.CO

Accepted Manuscript